



**HAL**  
open science

# Automatic surface remeshing of 3D structural models at specified resolution: A method based on Voronoi diagrams

Jeanne Pellerin, Bruno Lévy, Guillaume Caumon, Arnaud Botella

## ► To cite this version:

Jeanne Pellerin, Bruno Lévy, Guillaume Caumon, Arnaud Botella. Automatic surface remeshing of 3D structural models at specified resolution: A method based on Voronoi diagrams. *Computers & Geosciences*, 2014, 62, pp.103-116. 10.1016/j.cageo.2013.09.008 . hal-00924622

**HAL Id: hal-00924622**

**<https://inria.hal.science/hal-00924622>**

Submitted on 4 Mar 2016

**HAL** is a multi-disciplinary open access archive for the deposit and dissemination of scientific research documents, whether they are published or not. The documents may come from teaching and research institutions in France or abroad, or from public or private research centers.

L'archive ouverte pluridisciplinaire **HAL**, est destinée au dépôt et à la diffusion de documents scientifiques de niveau recherche, publiés ou non, émanant des établissements d'enseignement et de recherche français ou étrangers, des laboratoires publics ou privés.

# Automatic Surface Remeshing of 3D Structural Models at Specified Resolution: a Method Based on Voronoi Diagrams

Jeanne Pellerin<sup>a,c,b</sup>, Bruno Lévy<sup>b</sup>, Guillaume Caumon<sup>a</sup>, Arnaud Botella<sup>a,c,b</sup>

<sup>a</sup>*Géoressources (UMR 7359), Université de Lorraine-ENSG/CNRS/CREGU, Vandoeuvre-lès-Nancy, F-54500, France*

<sup>b</sup>*Inria - Project Alice, Villers-lès-Nancy, F-54600, France*

<sup>c</sup>*ASGA, Vandoeuvre-lès-Nancy, F-54500, France*

---

## Abstract

We propose a method to remesh the surfaces of 3D sealed geological structural models for subsequent volumetric meshing. The input of the method is a set of triangulated surfaces that are in contact along given lines and at given points. The output is a set of surfaces meshed with triangles as equilateral as possible. The method relies on a global Centroidal Voronoi optimization to place the vertices of the final surfaces combined with combinatorial considerations to either recover or simplify the surfaces, lines and points of the input model. When the final resolution is sufficient, the input contact lines, and points are also contact lines and points of the final model. However, when dealing with models with complex contacts, resolution may be insufficient and instead of a refinement strategy that may lead to too many points, we propose to locally merge some features of the input model. This ability to simplify the input model is particularly interesting when the model is to be volumetrically meshed. The method is demonstrated on twelve structural models, including seven models built with an implicit modeling method, and one folded layer model affected by a discrete fracture network.

*Keywords:* Remeshing, Structural Model, Non-manifold, Restricted Voronoi Diagram

---

## 1. Introduction

3D subsurface models have gained significant interest to optimize the management of natural resources and associated risks (Farmer, 2005). Among published techniques, 3D surfaces are often used to represent geological structures because they allow the modeling of many complex configurations encountered in nature. The various strategies to generate these models lead to several surfaces often defined by triangles (see Caumon et al. (2009) for a review). However triangle mesh quality and resolution may vary significantly depending on the modeler choices and on the algorithms involved during the model building. For instance, recent geomodeling methods use level-set (implicit) surfaces to account for various data types but produce very poor quality meshes (Calcagno et al., 2008; Collon-Drouaillet et al., 2012; Caumon et al., 2013). The mesh should therefore be adapted for applications such as the efficient visualization of very large models, the edition of the model geometry, for example when incorporating new data or when smoothing the model surfaces (e.g., Mallet, 2002), the restoration of 2D horizons (e.g., Dunbar and Cook, 2003), and 3D

---

Please cite this paper as: J. Pellerin, B. Lévy, G. Caumon, and A. Botella, Automatic surface remeshing of 3D structural models at specified resolution: A method based on Voronoi diagrams, *Computers & Geosciences*, vol. 62, no. 0, pp. 103–116, 2014, doi:10.1016/j.cageo.2013.09.008

---

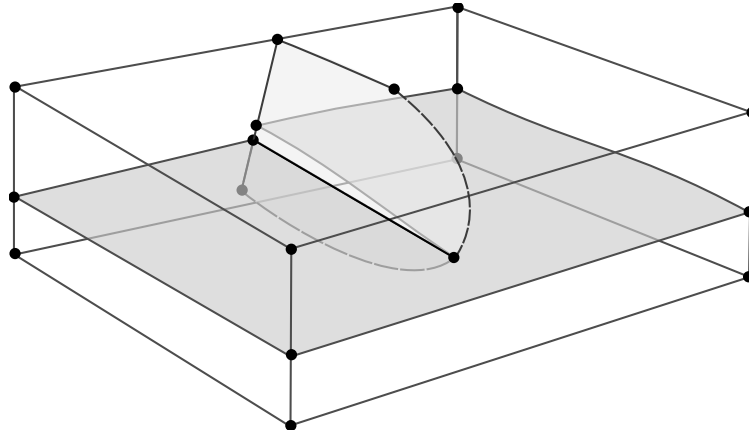


Figure 1: Surface structural model components. An horizon, cut by a normal fault, is included in a box. The surfaces are cut into several parts by the contact lines (full lines). Each contact line part has one triple point at its two extremities (black dots). The fault terminates laterally and has free boundaries (dashed lines).

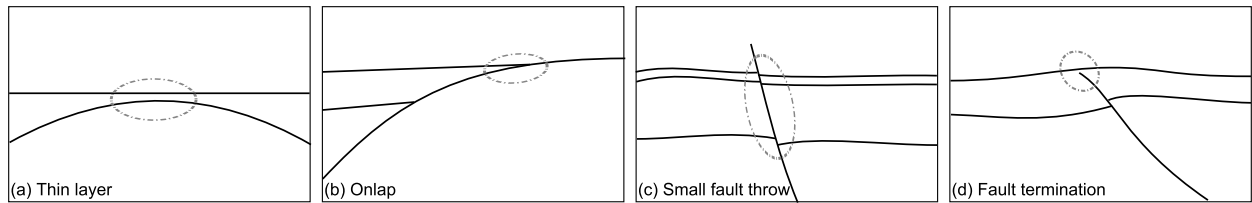


Figure 2: Cross-section view of the main meshing challenges in geological models

conformable gridding (e.g., [Prevost et al., 2005](#)). Remeshing the surfaces of a 3D structural model without altering its essential features is therefore an important step of the modeling process.

Most surface remeshing methods are developed for standalone closed surfaces (see [Alliez et al. \(2008\)](#) for a review) and cannot be used to globally remesh 3D structural models which have several interconnected surfaces (Fig. 1). Moreover there are three main challenges when remeshing a 3D structural model: (1) its surfaces can be very close (e.g., when bounding a thin layer Fig. 2a); (2) and they can intersect at small angles (e.g., when a layer pinches out laterally due to erosion Fig. 2b); (3) its contact lines may be very close as often observed for horizon cutoff lines on both sides of a fault surface (Fig. 2c) or on the tip of some syn-sedimentary faults (Fig. 2d). In these configurations, the first challenge is to honor the features smaller than required mesh element size while keeping the number of elements and their quality acceptable. The second challenge is to do that in a robust and accurate manner. Indeed, resampling a surface introduces geometrical approximations which may break the internal consistency of the model.

In this paper we propose a structural model remeshing method that produces a high-quality remesh of the model surfaces and of their intersections. Our method is based on the work of [Pellerin et al. \(2011\)](#). We introduce strategies to modify small-scale features of the input model so that the final model is adapted to the desired resolution and present detailed results on twelve 3D structural models that are remeshed at different resolutions and simplified when necessary.

### 1.1. Goals

*Input.* Geological models are constituted of several interconnected surface parts. Most of the time surface parts defining the zone of interest are also to consider (Fig. 1). These triangulated surface parts, the lines

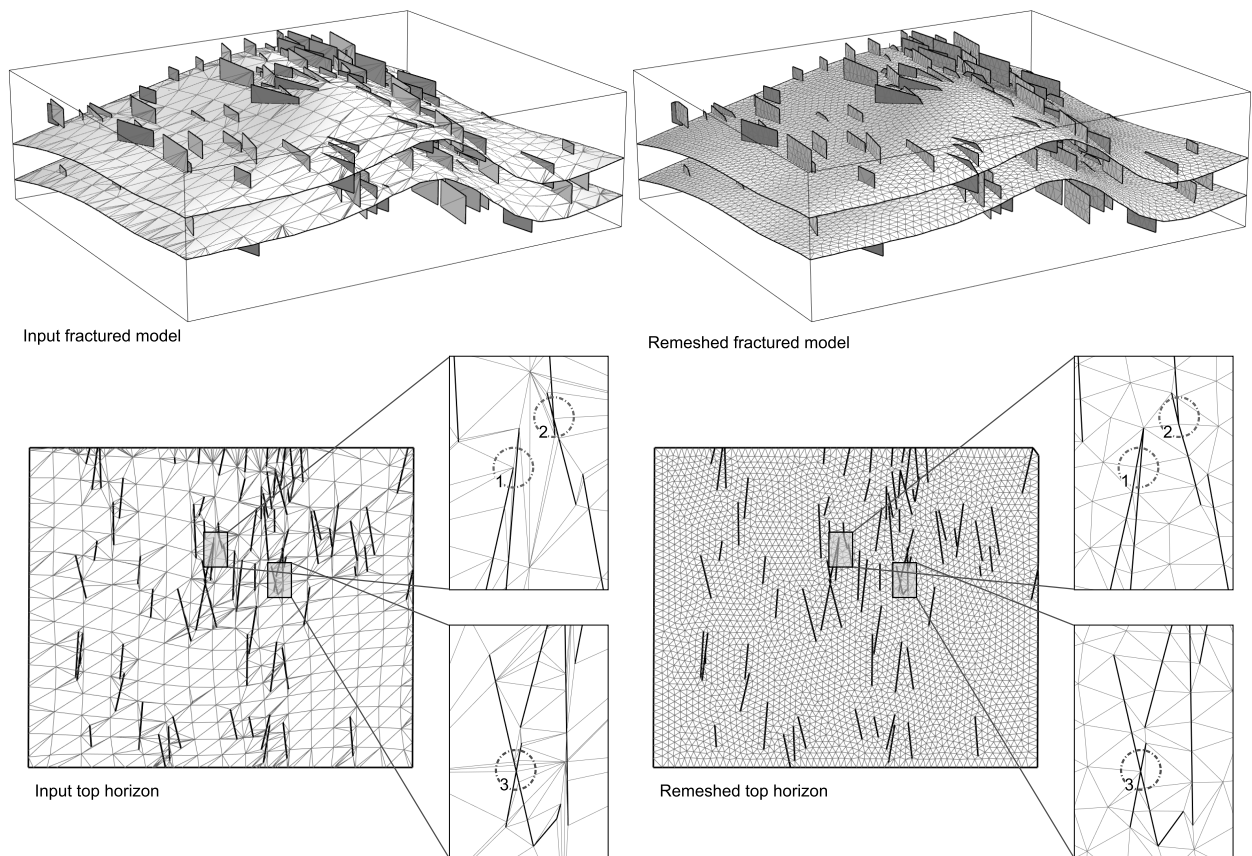


Figure 3: Remeshing a model with 200 fractures displaying challenging intersections. Quality of the remeshed surfaces is improved, three types of challenging intersections (1) slightly crossing fractures (2) almost intersecting fractures (3) low angle crossing, are remeshed and modified according to the desired resolution.

along which they intersect, and the extremities of these lines, called triple points in this paper, are the input of the method. Inconsistencies of the input model (non-water tightness, holes, non-conformal triangulation of the input surfaces along contact lines) are not handled.

*Output.* Our method computes a global remeshing of all the surfaces. The triangles of the output mesh are as equilateral as possible. Their quality does not depend on the input mesh quality and the method is resistant to degenerated triangles (skewed elements). The contacts between the surfaces are also remeshed and the surfaces remain conformal. Some modifications are done to simplify the model where contacts lines are too close (Fig. 3). This ability to simplify the input model is particularly interesting in the perspective of model gridding because distances between model features have a strong impact on gridding feasibility.

*Principle.* We use a Centroidal Voronoi Tessellation to place adequately a given number of points near the surfaces and contact lines of the model (section 3.1). A topological control is then used to determine the vertices and triangles of the final surface from the intersection of the Voronoi diagram of these points with the model while recovering the model components (section 3.2).

## 2. Background

### 2.1. Related work

The classical strategy to remesh a possibly high number of surfaces and their contact lines is to remesh them one by one. For example, [Lepage \(2003\)](#) and [Prevost et al. \(2005\)](#) propose to first remesh each contact line then parameterize each surface part to place it in a 2D space and remesh it with a constrained Delaunay refinement strategy. To ease the constrained Delaunay remeshing of surface parts, [Dey and Levine \(2009\)](#) protect the boundaries with balls of adaptive size in which no vertex can be inserted when remeshing surface parts.

Because these methods remesh independently the different surface and line parts of a model, they have to reach a sampling dense enough in areas where two surfaces are close or intersect at small angles to recover all the input parts (see also section 2.2.3). This makes the number of vertices of the output mesh difficult to control. To avoid adding too many points in these areas, [Pellerin et al. \(2011\)](#) propose to adapt the remeshing method of [Yan et al. \(2009\)](#) to geological models. The vertices of the final mesh are placed by minimizing a Centroidal Voronoi Tessellation objective function, an approach used to generate high quality meshes ([Lloyd, 1982](#); [Du et al., 1999](#); [Alliez et al., 2005](#); [Valette et al., 2008](#); [Yan et al., 2009](#); [Levy and Liu, 2010](#); [Chen et al., 2012](#)). Then, they locally recover the different connected components of the model (surface parts, contacts, and triple points) by adding one point per connected component. This simple strategy is very efficient to remesh thin layers and parallel contact lines, but fails when the resolution is not sufficient to capture other small-scale features in particular close triple points. A solution is then to modify these features, and that means to modify the model topology.

Remeshing methods that allow topological changes can be grouped in two main categories: those doing local modifications and those operating globally. The local modifications proposed by [Garland and Heckbert \(1997\)](#) generalize edge contractions and perform both close vertex contraction and edge contraction at the same time. Vertex clustering, introduced by [Rossignac and Borrel \(1993\)](#), was used to remesh discrete fractures network by [Mustapha et al. \(2011\)](#). A fixed size box scans the initial model in the three directions and the vertices inside it are replaced by a single vertex placed at the center of the box. Methods operating globally consider the entire model for the simplifications and subdivide into cells whose dimensions control the degree of simplification. For closed surfaces, [Andujar et al. \(2002\)](#) use an octree, flag each cell as inside or outside the surface, and reconstruct a simplified closed surface from the remaining cells. Considering

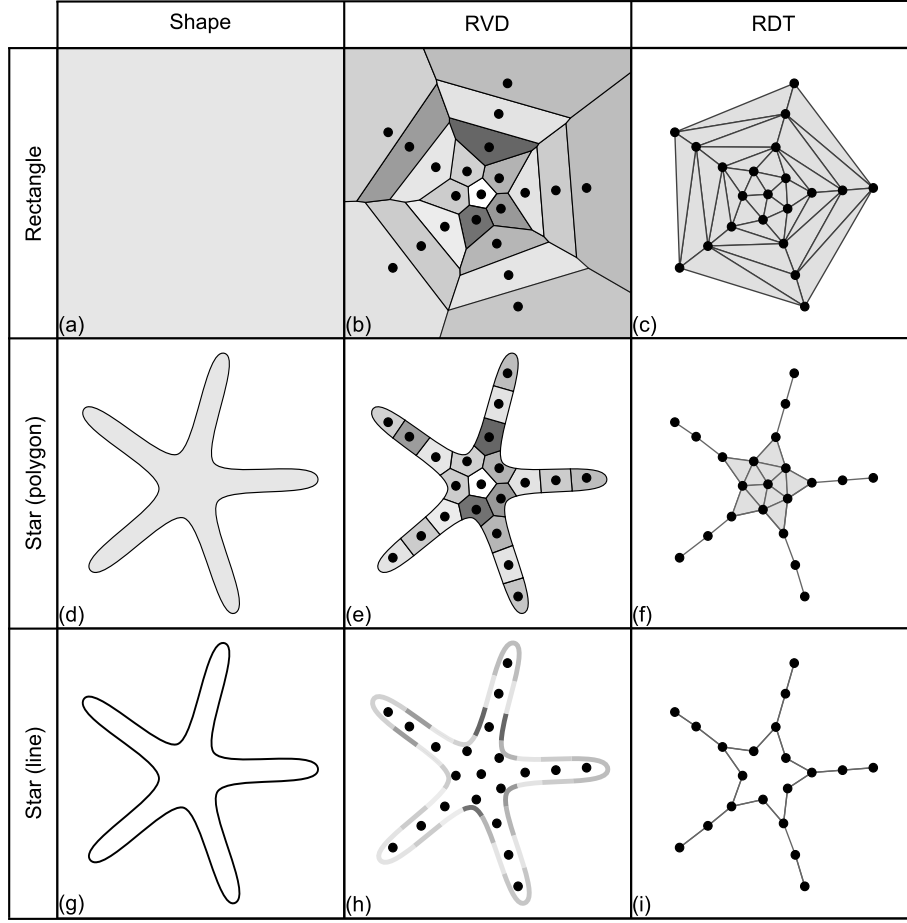


Figure 4: Restricted Voronoi diagrams and dual restricted Delaunay triangulations to three shapes. The restricted Voronoi diagram to the rectangle (b) is the Voronoi diagram of the seeds (black dots) where infinite cells and edges are clipped, and (c) is also the Delaunay triangulation of the seeds.

globally the model and working with a volumetric subdivision of the space permit to analyze locally the relationships between its different parts. In this paper we propose a similar idea, except that a Voronoi diagram determines the space partitioning.

## 2.2. Key concepts and definitions

### 2.2.1. Voronoi Diagram and Restricted Voronoi Diagram

A Voronoi diagram is defined relatively to set of points called seeds, and denoted  $S$  (e.g., [Aurenhammer, 1991](#)). To each seed  $p \in S$  corresponds a Voronoi cell: the set of points of the space closer to this seed than to any other seed (Fig. 4b). In  $\mathbb{R}^3$ , if we consider the Euclidean distance  $\|\cdot\|$ , the Voronoi cell of  $p$  is defined as  $V_p = \{x \in \mathbb{R}^3 \mid \|px\| \leq \|qx\|, q \in S\}$ .

The restricted Voronoi diagram of the seeds  $S$  to any object  $\Omega$  is the intersection of the Voronoi diagram of the seeds with this object (Fig. 4e and 4h). The intersection of the Voronoi cell  $V_p$  with  $\Omega$  is called the restricted Voronoi cell of  $p$  to  $\Omega$  and is defined as  $V_{p \cap \Omega} = V_p \cap \Omega$ . Because the Voronoi diagram is a partition of the considered space, the restricted Voronoi diagram to any object  $\Omega$  contained in that space is a partition of that object.

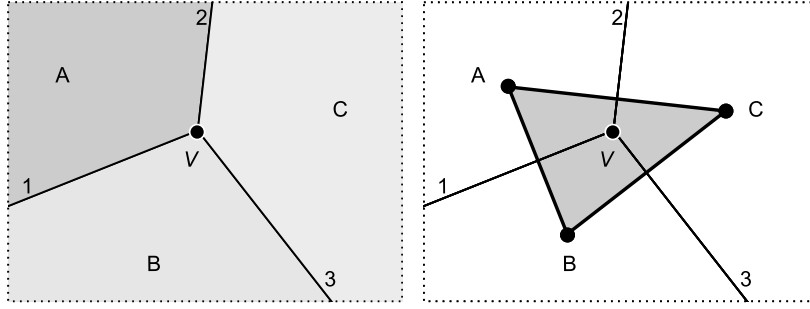


Figure 5: 2D Voronoi-Delaunay dual relationship.  $V$  is a vertex shared by 3 Voronoi cells:  $A$ ,  $B$ , and  $C$ . There is one point per cell, one edge per edge common to two cells, and one triangle  $ABC$  for  $V$ .

### 2.2.2. Delaunay Triangulation and Restricted Delaunay Triangulation

The Delaunay triangulation of a set of seeds  $S$  is the geometric dual of the Voronoi diagram of  $S$ . In 2D, there is one edge in the Delaunay triangulation for each edge of the Voronoi diagram shared by two cells, and one triangle for each vertex of the Voronoi diagram shared by three cells (Fig. 4c).

The Restricted Delaunay Triangulation (Edelsbrunner and Shah, 1997), dual of the restricted Voronoi diagram, is defined like the Delaunay triangulation. For a restricted Voronoi diagram to a surface, there is one edge in the restricted Delaunay triangulation for each edge shared by two restricted Voronoi cells, and one triangle for each vertex shared by three restricted Voronoi cells (Fig. 4f and 4i). For an object  $B$  such that  $B \subset \Omega$ , the restricted Voronoi diagram of the seeds  $S$  to  $B$  is included in the restricted Voronoi diagram of  $S$  to  $\Omega$ , and the restricted Delaunay triangulation of  $S$  to  $B$  is a subset of the restricted Delaunay triangulation of  $S$  to  $\Omega$ . An example is given Fig. 4, where the segments remeshing the star contour (Fig. 4i) are included in the remesh of the star (Fig. 4f).

### 2.2.3. Input surface and Restricted Delaunay Triangulation

The restricted Delaunay triangulation of given seeds to an input surface remeshes this surface. However, it does not necessarily have the same topology as the input surface (not homeomorphic), see for example the restricted Delaunay triangulation to the star on Fig. 4f. To ensure that the restricted Delaunay triangulation is homeomorphic to an input manifold surface it is sufficient to verify the topological ball property (Edelsbrunner and Shah, 1997): all the restricted Voronoi cells (respectively facets and edges) of  $S$  to  $\Omega$  are topological disks (respectively segments and points) and all the restricted Voronoi cells (respectively facets and edges) of  $S$  to the boundary of  $\Omega$  are topological segments (respectively points and the emptyset). A geometrical means to enforce the topological ball property is to have an  $\varepsilon$ -sampling of the input surface (Amenta and Bern, 1999): if for each point  $x$  of the surface  $\Omega$ , there is a seed of  $S$  at a distance smaller than  $\varepsilon \times lfs(x)$ , where  $\varepsilon < 0.3$  and  $lfs$  denotes the local feature size (distance to the medial axis of  $\Omega$ ).

In practice these conditions are difficult to enforce when the final number of vertices is fixed and we try to ensure a weaker condition (section 3.2).

## 3. Surface remeshing method

This section details the two main steps of our surface remeshing method: the optimization of a given number of seeds on the model (section 3.1) and the building of the final mesh from the connected components of the restricted Voronoi diagram of the seeds (section 3.2).

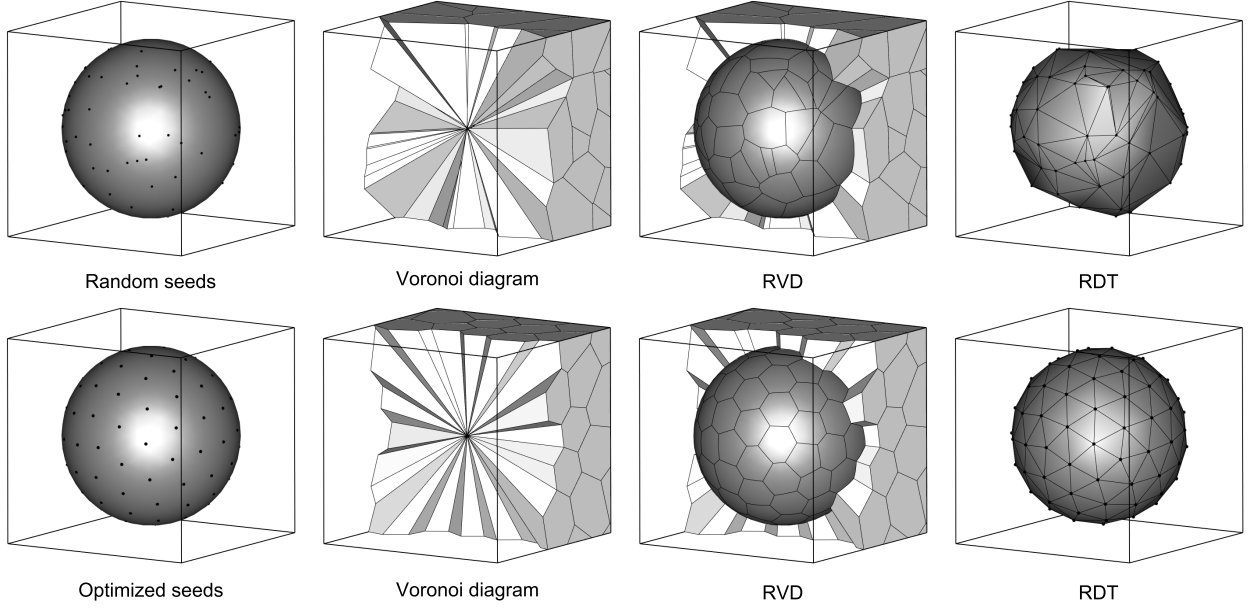


Figure 6: Optimization of 100 seeds on a sphere. After optimization the restricted Voronoi diagram has compact well-shaped cells and the restricted Delaunay triangulation has almost equilateral triangles.

### 3.1. Optimization of seed positions

First, a fixed number of seeds are placed so that they are a good sampling of the geological model. Each seed samples the model in the sense that it represents the part of the model closest to it than to any other seed. The input number of seeds then determines the resolution at which the model will be remeshed, it may be computed from the square root of the model area divided by the target edge length. The restricted Voronoi diagram of the seeds to the geological model partitions this model and associates to each seed a small part of this model. The goal is then to have restricted Voronoi cells that are well-shaped (i.e. dual triangles are well shaped), have the same importance (area), and are compact (Fig. 6). These properties are reached when the restricted Voronoi diagram of the seeds is centroidal.

*Restricted Centroidal Voronoi Diagram.* A Voronoi diagram is centroidal if each seed is located at the centroid of its Voronoi cell (Du et al., 1999). A restricted Voronoi diagram is centroidal if each seed  $p$  is at the centroid of its restricted Voronoi cell,  $V_p \cap \Omega$  (Du et al., 2003; Yan et al., 2009). The centroid  $p^*$  of a domain  $A$  is defined from a density function  $\rho$  by:

$$p^* = \frac{\int_A y \rho(y) dy}{\int_A \rho(y) dy} \quad (1)$$

The restricted centroidal Voronoi diagram can be computed by optimizing the positions of a given number of points randomly placed on the input surface. The most intuitive method, Lloyd's algorithm, moves iteratively each seed to the centroid of its restricted Voronoi cell. Liu et al. (2009) propose to compute it with a faster Newton-like algorithm since a centroidal Voronoi diagram can be defined as a critical point of the objective function  $F_{CVT}$ :

$$F_{CVT}(S) = \sum_{p \in S} \int_{V_p \cap \Omega} \rho(y) \|y - p\|^2 dy \quad (2)$$

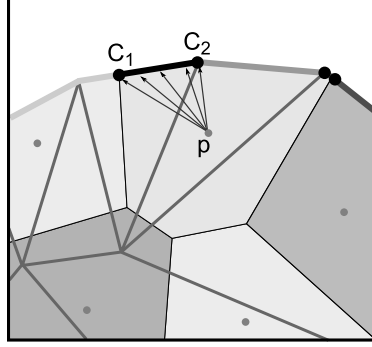


Figure 7: Integration segments for the computation of the border energy

where  $S$  is the set of seeds,  $V_p \cap \Omega$  is the Voronoi cell of seed  $p$  restricted to  $\Omega$ , and  $\|\cdot\|$  the Euclidean distance. This function is  $C^2$  except when two seeds coincide (Zhang et al., 2012) or when a bisector coincides with a boundary facet plane (Liu et al., 2009), however practical results show the applicability of the Newton-like method (e.g., Yan et al., 2009).

*Boundary sampling.* When computing a restricted centroidal Voronoi diagram to a surface that has a boundary, optimized seeds are not on the boundary because the centroid of a cell intersecting a boundary line is not on this line. To modify this stable position, a border energy term can be added to the objective function for seeds whose Voronoi cell ( $V_p$ ) intersects the boundary ( $B$ ):

$$F_B(S) = \sum_{p \in S} \left[ \int_{V_p \cap B} \|y - p\| dy \right]^2 \quad (3)$$

To evaluate this function and its gradient we decompose the restriction of each Voronoi cell to the boundary ( $V_p \cap B$ ) into segments (Fig. 7). For each segment,  $E = C_1 C_2$ , we denote  $\vec{N} = \overrightarrow{C_2 p} \cdot \overrightarrow{C_2 C_1}$  and we have  $F_B^E = 1/2 \|\vec{N}\|^2$ , that is the square area of the triangle  $p C_1 C_2$  (Fig. 7). The corresponding gradient is:

$$\frac{dF_B}{dS}(p, C_1, C_2) = \frac{dF_B}{dp} + \frac{dF_B}{dC_1} \frac{dC_1}{dS} + \frac{dF_B}{dC_2} \frac{dC_2}{dS} \quad (4)$$

where  $dF_B/dp = \vec{N} \times \overrightarrow{C_1 C_2}$ , the terms  $dF_B/dC_1$  and  $dF_B/dC_2$  are evaluated similarly. The term  $dC/dS$  depends on point  $C$  configuration. Either  $C$  is a vertex of the initial mesh and the gradient is a null vector, or  $C$  is at the intersection of the bisector between seeds  $p_0$  and  $p_1$  with an edge of an initial triangle and is computed as:

$$\frac{dC}{dS} = \begin{pmatrix} [p_1 - p_0]^t \\ [N_1]^t \\ [N_2]^t \end{pmatrix}^{-1} \begin{pmatrix} [C - p_0]^t & [p_1 - C]^t \\ [C - p_0]^t & 0 \\ 0 & 0 \end{pmatrix} \quad (5)$$

where  $N_1$  and  $N_2$  are the normals to two planes built so that they intersect along a line containing the segment  $C_1 C_2$ . The proof is given in Levy and Liu (2010). To improve the placement of the seeds near boundaries and contact lines we minimize the objective function  $F = (1 - \alpha)F_{CVT} + \alpha F_B$  where  $\alpha$  is the ratio between the boundary energy and CVT energy gradient norms.

**Data:** a model  $\Omega$ , the desired number of points  $n$

**Result:** an isotropic sampling  $\mathbf{S}$  of  $\Omega$

(1)  $\mathbf{S} \leftarrow$  initial random sampling of  $\Omega$  (Levy and Bonneel, 2013) ;

**while** *minimum not reached* **do**

    (2) Compute the restricted Voronoi diagram of  $\mathbf{S}$  to  $\Omega$  (Levy and Bonneel, 2013) ;

    (3) Compute  $F(\mathbf{S})$  and  $dF/d\mathbf{S}$  (Liu et al., 2009) ;

    Determine the search direction  $\Delta\mathbf{S}$  (Liu et al., 2009) ;

$\mathbf{S} \leftarrow \mathbf{S} + \Delta\mathbf{S}$  ;

**end**

**Algorithm 1:** Optimization of the seeds

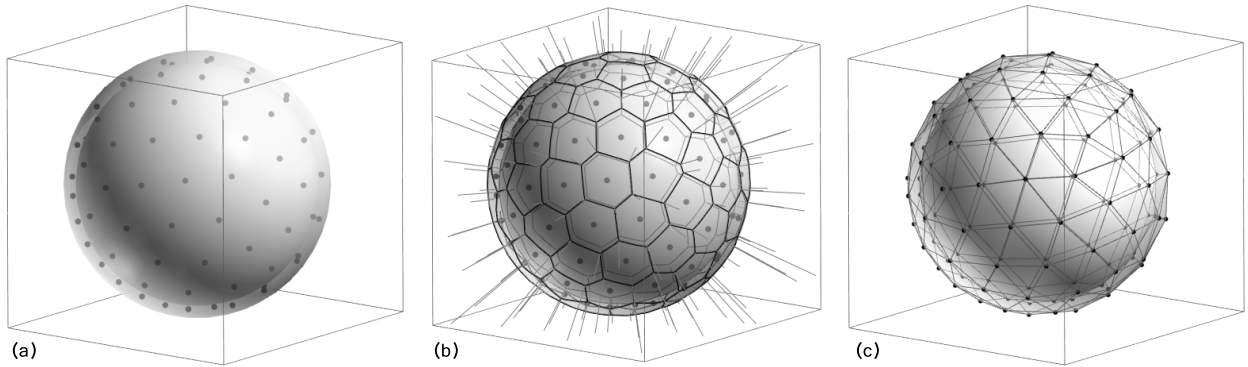


Figure 8: Nested spheres remeshing. (a) 100 optimized seeds are sandwiched between two spheres (b) Each restricted Voronoi cell has 2 connected components (c) Dual of the connected components of the restricted Voronoi diagram (see Fig. 9).

*Implementation.* Algorithm 1 summarizes the steps to perform the optimization of a given number of seeds over a model  $\Omega$ . (1) The initial random placement of the seeds on the model surfaces is done using the algorithm given by Levy and Bonneel (2013). (2) The computation of the restricted Voronoi diagram is done using the fast parallelized method also described by Levy and Bonneel (2013). (3) The contributions of each cell of the restricted Voronoi diagram to the objective function and to its gradient is computed following Yan et al. (2009) for the CVT energy and the above for the boundary term. The minimization of the objective function  $F$  is done with a L-BFGS algorithm (Nocedal, 1980). The optimization can be stopped when the norm of the gradient is inferior to a given value. From our experience, convergence is very fast, and in practice we stop the optimization process after 100 iterations. Specific convergence rates are discussed by Liu et al. (2009). In all the cases we considered the input mesh resolution does not impact the convergence while increased feature density slightly decreases the convergence.

### 3.2. Mesh Building

Once the seeds have been optimally distributed, we compute their restricted Voronoi diagram to the structural model and compute the connected components of the restricted Voronoi cells to determine the vertices and triangles of the output mesh.

*Surface part remeshing.* Let's first consider a (non-geological) model in which the different surface parts do not intersect and have no boundary. An example with two nested spheres is given Fig. 8. The two surface parts are sampled by 100 seeds whose optimized positions are between the spheres (Fig. 9a). To recover the input surface parts, each seed is replaced by two vertices, one for each connected component of the restricted

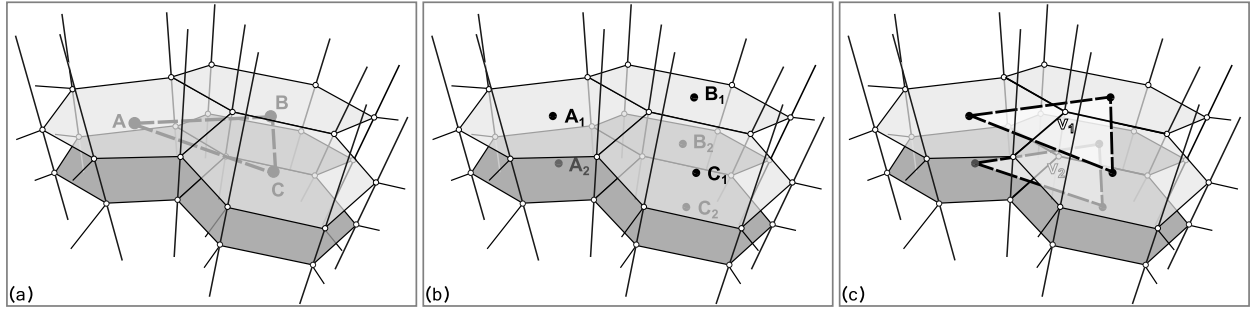


Figure 9: Remeshing two close surfaces. (a) 3 seeds (**A**, **B** and **C**) are sandwiched between two close surfaces, their restricted Voronoi cells have two connected components, but in the dual restricted Delaunay triangulation there is only one triangle **ABC**. (b) Each seed is replaced by two points. (c) Two triangles  $A_1B_1C_1$  and  $A_2B_2C_2$  are built corresponding to the points  $v_1$  and  $v_2$  shared by three restricted cell connected components.

Voronoi cell (Fig. 9b). There is then one triangle to build for each point shared by three restricted Voronoi cells (Fig. 8c and 9c). The obtained mesh is a dual of the connected components of the restricted centroidal Voronoi diagram, it is closer to the input mesh than the restricted Delaunay triangulation (one sphere in this case). The multi-nerve theorem gives that it is homotopy equivalent to the input model (Colin de Verdiere et al., 2012).

*Contact line remeshing.* Now, we consider a surface that has a boundary. Similarly to what happens for surface parts, the boundary may not be correctly remeshed if the number of seeds is too small, see the branches of the star on Fig. 4f. To remesh them correctly, each seed is replaced by as many points as the number of connected components of the intersection between its Voronoi cell and the boundary lines (Fig. 10).

These additional points complicate the triangle building step since one connected component of one restricted Voronoi cell may correspond to several points (Fig. 10b). As a consequence, the dual of points shared by three cells may not be a triangle (see the gray points on Fig. 10c & d), and additional polygons, dual of the edges shared by two cells and intersecting twice the boundary, should be built between close boundary lines (see the gray segments on Fig. 10c & d).

The more intersections between the restricted Voronoi cell and the model boundary, the more vertices in this cell. This may lead to configurations where the polygons to build intersect (Fig. 11a). To avoid this, if there are more than two points for a connected component of a restricted Voronoi cell, they are merged. This makes our method more robust, but at the cost of modifications of the surface connections that are questionable from a geological point of view and depend highly on the optimized seed positions.

*Triple point remeshing.* The last elements to take into account for geological model remeshing are triple points, i.e. points at the intersection of at least two contact lines (Fig. 1). To recover all the triple points of the input model there is no other option than to put one point for each triple point present in the restricted Voronoi cell. So, to fully reconstruct the input model, we need to have for each restricted Voronoi cell one point per triple point, one point per contact, and one point per surface part (see Algorithm 3).

When there are more than one triple point on a connected component of a restricted Voronoi cell to the boundary, i.e. the final resolution is not sufficient, we choose to not recover all the triple points of the input model and we merge them (Fig. 11b). When this merging operation is done, the previously described merging is also performed. This way, each restricted Voronoi cell part has 1 or 2 points and the quads or triangles to build with these points do not intersect. The last modification is the merging of the vertices that

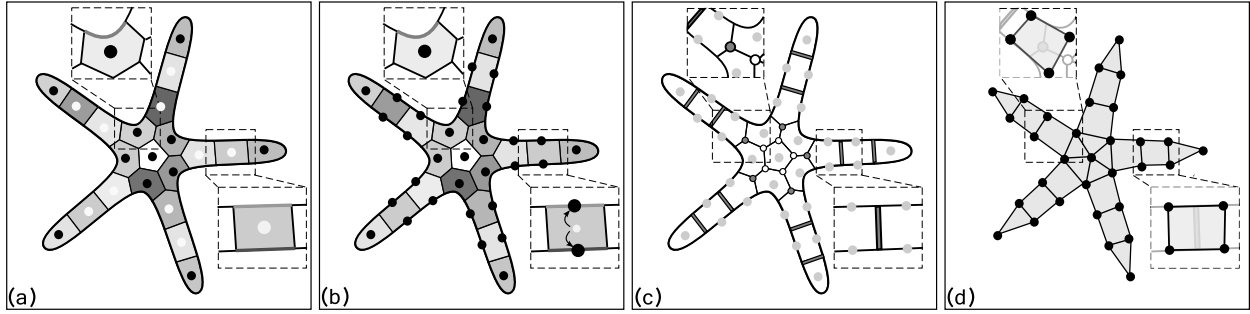


Figure 10: Remeshing a surface with a boundary. (a) 21 seeds sample the star; Voronoi cells of the white seeds intersect twice the boundary, those of the black seeds intersect it once or not at all. (b) Each white seed is replaced by two points, one per intersection of the cell with the boundary (c) The elements dual of the polygons of the final mesh are: regular restricted Voronoi vertices (white), restricted Voronoi vertices neighboring at least a restricted Voronoi cell with two points (gray), and the segments on the restricted Voronoi edges intersecting twice the boundary. (d) Final mesh is made of regular Delaunay triangles and quads.

**Data:** the restricted Voronoi diagram of optimized seeds  $S$  to the model  $\Omega$

**Result:** a triangular remesh of the model  $\Omega$

**foreach**  $i \in S$  **do**

- (1) Compute the connected components of the restricted Voronoi cell ;
- (2) Compute the points remeshing the cell ;

**end**

- (3) Build triangles ;

**Algorithm 2:** Output mesh building steps

correspond to close features, close meaning that the distance between them is inferior to a specified input value (Fig. 11c & d). This is a way to make the model easier to mesh and simplify very small features by removing small fault throws and joining fault tips close to another fault.

*Implementation.* Algorithm 2 summarizes the implementation of the mesh building steps. The input of the method is a restricted Voronoi diagram, a polygonal surface obtained from the intersection of the input model with the Voronoi diagram of the optimized seeds. Each polygon of the restricted Voronoi diagram is the intersection of one triangle of the input model and one Voronoi cell whose ids are known. (1) Each restricted Voronoi cell and its connected components are built using that information. (2) The vertices to put for each restricted Voronoi cell are computed following Algorithm 3. (3) The last step is to build the polygons linking these vertices (Fig 10).

### 3.3. Mesh Improvements

The quality of the triangles of the final mesh is completely dependent on the shape of the connected components of the restricted Voronoi cells. When they are close to regular hexagons the dual triangles are close to being equilateral, but relatively small triangular components might appear on the restricted Voronoi diagram when a Voronoi point or edge is close to one of the input surface. When such a facet is in the interior of the surface part it results in a valence three vertex that can be easily removed. When it is on a free boundary, the corresponding triangle is degenerated and is simply removed. When this facet is along a contact, the dual is also a degenerated triangle but a specific processing is necessary to remove it while maintaining the contact sealed. Removing these needle-shaped triangles corresponds to ignoring a small intersection of the Voronoi diagram with the input surface and can be seen as the result of the remeshing

**Data:** the restricted Voronoi cell of seed  $i$ , distance  $d_{resolution}$

**Result:** set of points remeshing the cell

```
foreach Connected component CC do  
  | if CC intersects boundary lines then  
  | | foreach Boundary connected component BC do  
  | | | if BC contains triple points then  
  | | | | Add a point per triple point ;  
  | | | else  
  | | | | Add a point on the boundary part BC ;  
  | | | end  
  | | end  
  | else  
  | | Add a point at the centroid of the connected component CC ;  
  | end
```

**end**

(2) Cluster and merge points sampling triple points connected by a boundary line (Fig. 11b) ;

(3) **foreach** *Connected component CC* **do**

```
  | if number of points  $\geq 2$  (Fig. 11a) then  
  | | Merge the points ;
```

```
  | end
```

**end**

(4) Cluster and merge the points whose corresponding model parts are close ( $d_{min} \leq d_{resolution}$ ) (Fig. 11c & d) ;

**Algorithm 3:** Output mesh vertex computation

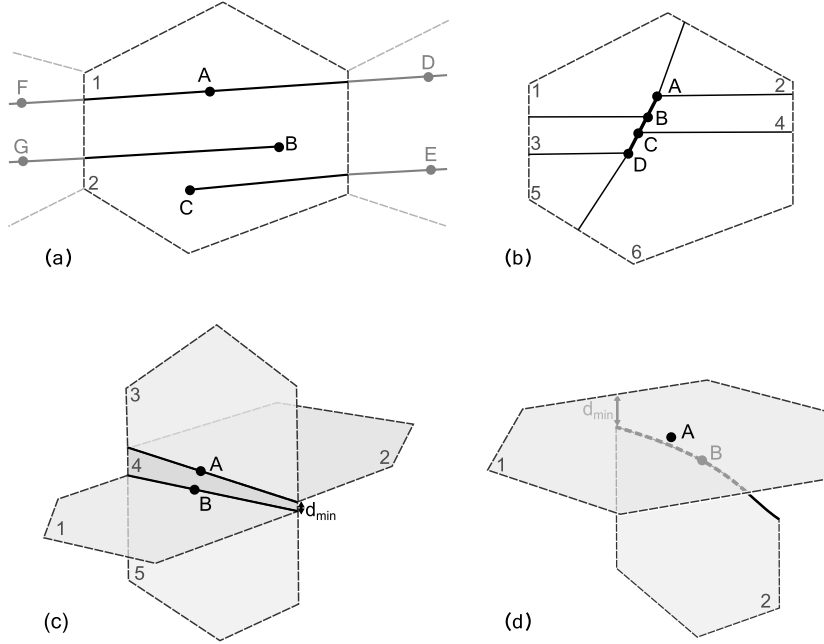


Figure 11: Configurations leading to modifications of the model. (a) The central restricted Voronoi cell component has 3 points (**A**, **B**, **C**), the polygons to build with these points **ABGF** and **ADEC** intersect. The modification proposed is to merge these 3 points. (b) Contact lines (black lines) cut this cell into 6 connected components. The 4 triple points (**A**, **B**, **C**, and **D**) will be merged because boundary segments link them. (c & d) If  $d_{min}$  is inferior to the given resolution, points **A** and **B** are merged.

if the input surface and/or the contacts lines were slightly moved so that the small facet on the restricted Voronoi diagram disappears.

As we use the Euclidean distance to approximate the geodesic distance (the length of the shortest path on the surface between two points) when sampling the surfaces and making some simplifications, triangles of the output mesh might intersect. They must be identified and the intersections must be resolved by vertex displacements or edge flipping.

#### 4. Results

We have applied our surface remeshing method on twelve structural models described in Table 1 (Figs. 12 to 20). The models are presented in an increasing meshing difficulty order. The non-faulted models are more easily remeshed than the faulted ones, however their stratigraphy may prove very challenging because of thin curved layers whose thicknesses vary. The difficulty to remesh fractured or faulted models depends on four factors: the number of faults, the number of intersections between faults, the number of faults terminating in the model, and throw sizes.

Input mesh sizes vary from several thousand triangles to almost one million triangles. Computation times to optimize the seed positions (100 iterations) and build the final mesh range between 13s and 150s on a 8-core laptop, depending mainly on the size of the input mesh and on the number of seeds. The input and final triangle quality are compared using three criteria: the smallest angle, the percentage of angles under 30 degrees, and the average triangle quality. The quality of a triangle is taken as  $Q = 6S/(\sqrt{3} h_{max} p)$  where  $S$  is the area of the triangle,  $h_{max}$  the length of its longest edge, and  $p$  its half perimeter (Frey and Borouchaki, 1999). Note that the output quality of the triangles is neither fixed

<b>Dataset</b>	<b>Horizons</b>	<b>Faults</b>	<b>Main challenges</b>	<b>Credentials</b>	<b>Figures</b>
<b>Coal veins</b> <i>10.2km × 1.3km × 280m</i>	29	0	Thin layers	Courtesy of Gocad consortium	Fig. 12
<b>Forward</b> <i>110m × 65m × 40m</i>	7	0	Thin layers, onlaps	Laurent (2013)	Fig. 13
<b>Detachment</b> <i>22km × 14km × 7.7km</i>	8	1	Thin layers	Courtesy of Chevron Guzofski et al. (2009)	Fig. 14
<b>Leipzig</b> <i>1.2km × 1.2km × 0.4km</i>	2	9	Fault network	Courtesy of Total	Fig. 14
<b>Lambda</b> <i>6km × 4.5km × 1.9km</i>	2	13	Low angle faults fault throws	Courtesy of Gocad consortium	Fig. 14
<b>DFN</b> <i>13km × 11km × 4km</i>	2	200	Fracture relations	Courtesy of Gocad consortium	Fig. 15 and 3
<b>HC</b> <i>18km × 10km × 10.2km</i>	7	2	Thin layers, Inverse fault	Courtesy of Harvard-Chevron	Fig. 15
<b>Cloudspin</b> <i>14.7km × 12km × 2km</i>	3	10	Low angle faults, fault throws	Courtesy of PDGM and Schlumberger	Fig. 16
<b>Clyde</b> <i>12km × 10.3km × 1.7km</i>	4	22	Fault intersections, fault throws	Confidential	Fig. 17 and 18
<b>Nancy</b> <i>11km × 3km × 1.4km</i>	7	26	Complex faults, fault throws	Courtesy of Total	Fig. 19
<b>Annot</b> <i>11km × 5.5km × 2.8km</i>	9	3	Thin layers, onlap, fault throws	Salles et al. (2011)	Fig. 20
<b>Sandbox</b> <i>3.5km × 3km × 0.5km</i>	8	33	Fault throws	Courtesy of IFPEN Colletta et al. (1991)	Fig. 20

Table 1: Main features and challenges of the 12 remeshed models

beforehand, nor does it depend on the quality of the input mesh. The Hausdorff distance between the output and input model is computed with the code of [Aspert et al. \(2002\)](#) and is given in percentage of the boundary box diagonal. The Hausdorff distance is a measure of how close the final model is of the initial one and is classically used to evaluate surface remeshing methods. For two subsets  $X$  and  $Y$  it is defined as  $d_H(X, Y) = \text{Max} \{ \text{Max}_{p_1 \in X} (\text{Min}_{p_2 \in Y} (d(p_1, p_2))) \mid \text{Max}_{p_2 \in Y} (\text{Min}_{p_1 \in X} (d(p_2, p_1))) \}$ . The output models are visually similar to the input ones. Detailed statistics on the input and output meshes are given in [Table 2](#). The largest features are recovered whereas some small features, with regard to the resolution of the Voronoi diagram, may be altered. This is illustrated by the differences in the numbers of surface parts, contacts, and triple points between the input and remeshed models ([Table 2](#)).

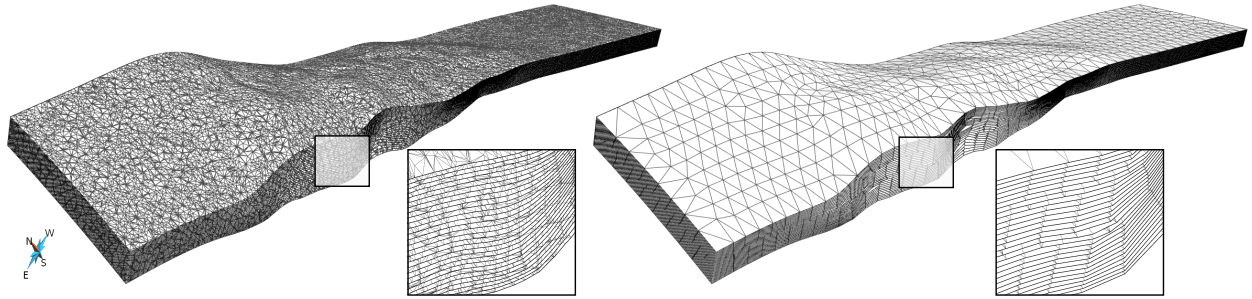


Figure 12: Coal veins remeshing. 29 sub-vertical surfaces delimit thin coal veins. 1000 seeds are sufficient to remesh the model decreasing the number of triangles from nearly one million to 35 thousand (see Tables 1 and 2 for details).

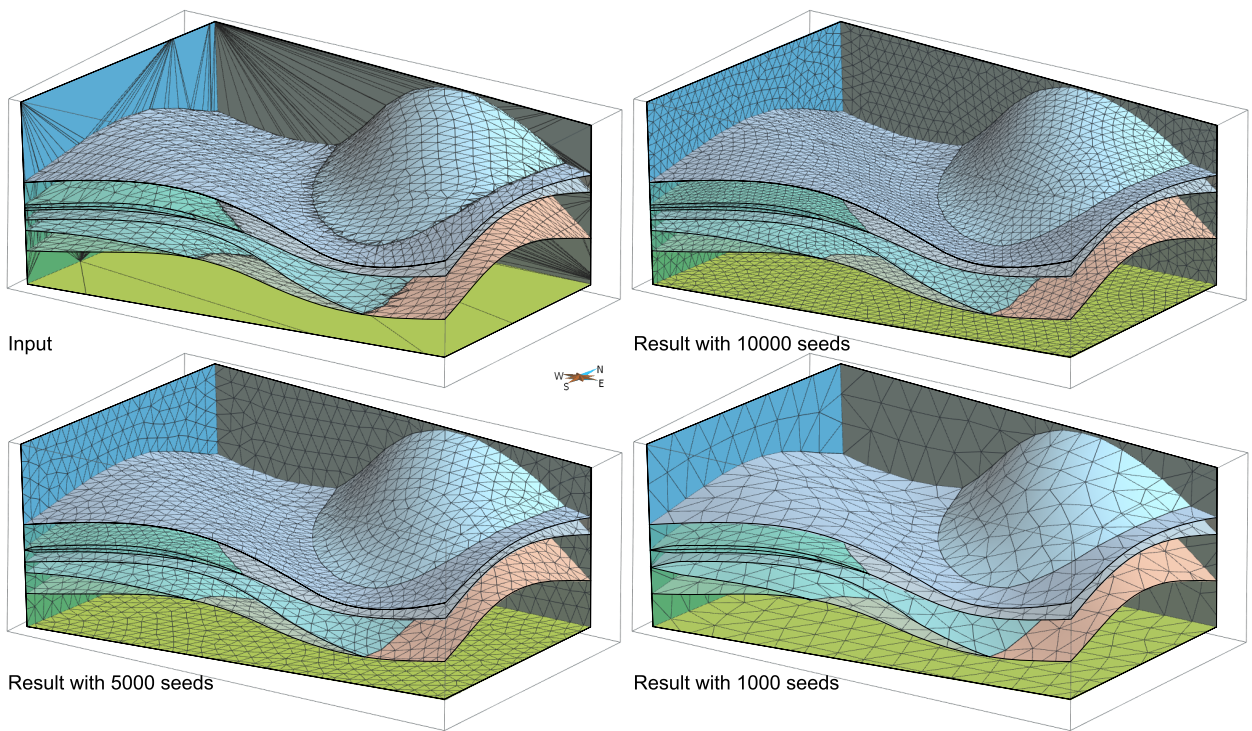


Figure 13: Forward model remeshing with varying resolutions. Input model shows 3 three challenges for remeshing, very thin layers, major layer thickness variations and low-angle contacts between horizons due to onlapping geometries (see Tables 1 and 2 for details).

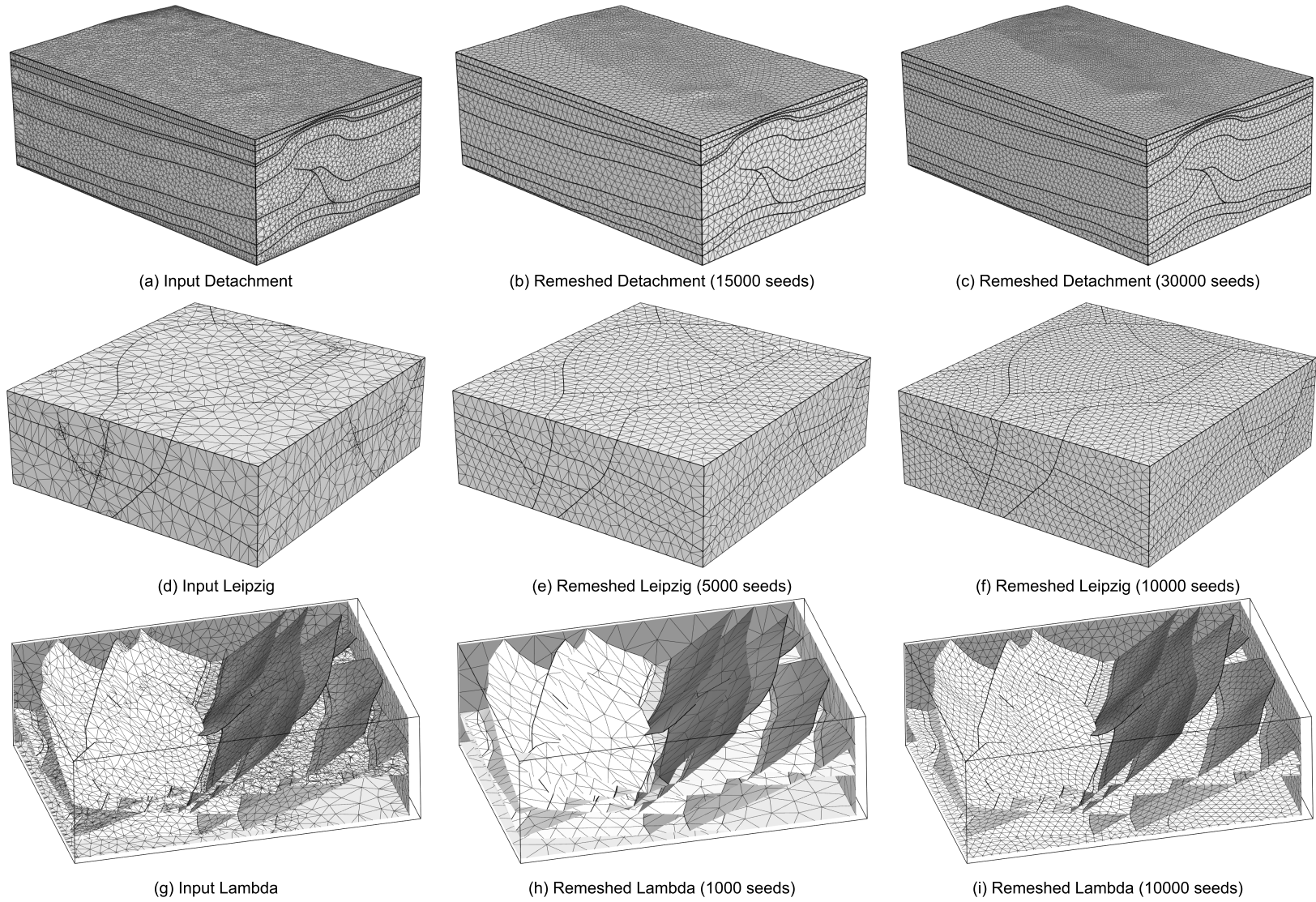


Figure 14: Remeshing the Detachment, Leipzig, and Lambda models (see Tables 1 and 2 for details).

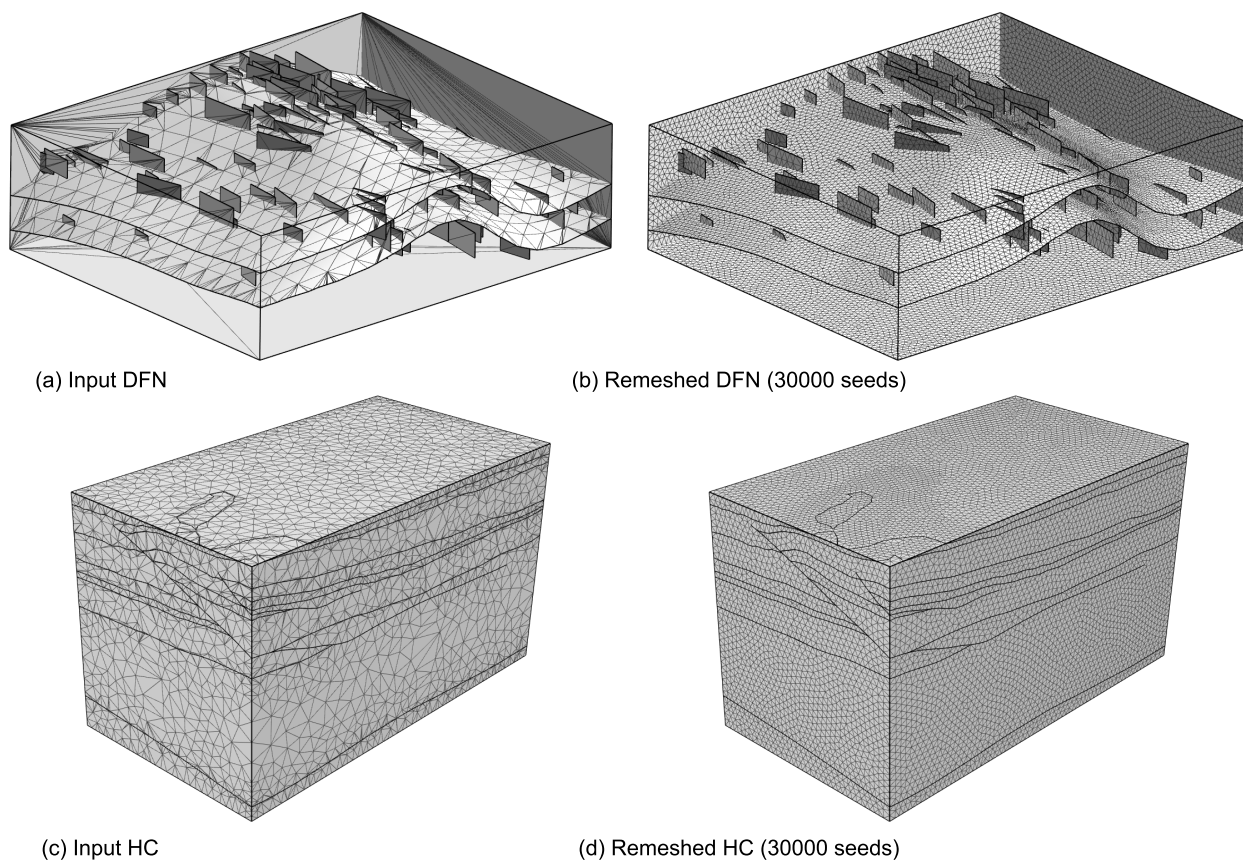


Figure 15: Remeshing the DFN and HC models (see Tables 1 and 2 for details)

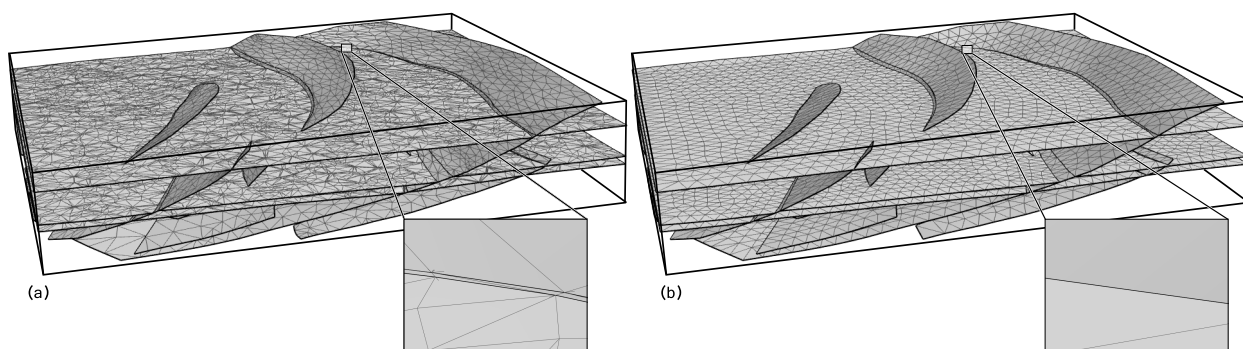


Figure 16: Cloudspin model remeshing. (a) Input model with very small throw near fault ends. (b) Output surfaces, remeshing was done with 5000 seeds, contact lines are locally merged (see Tables 1 and 2 for details).

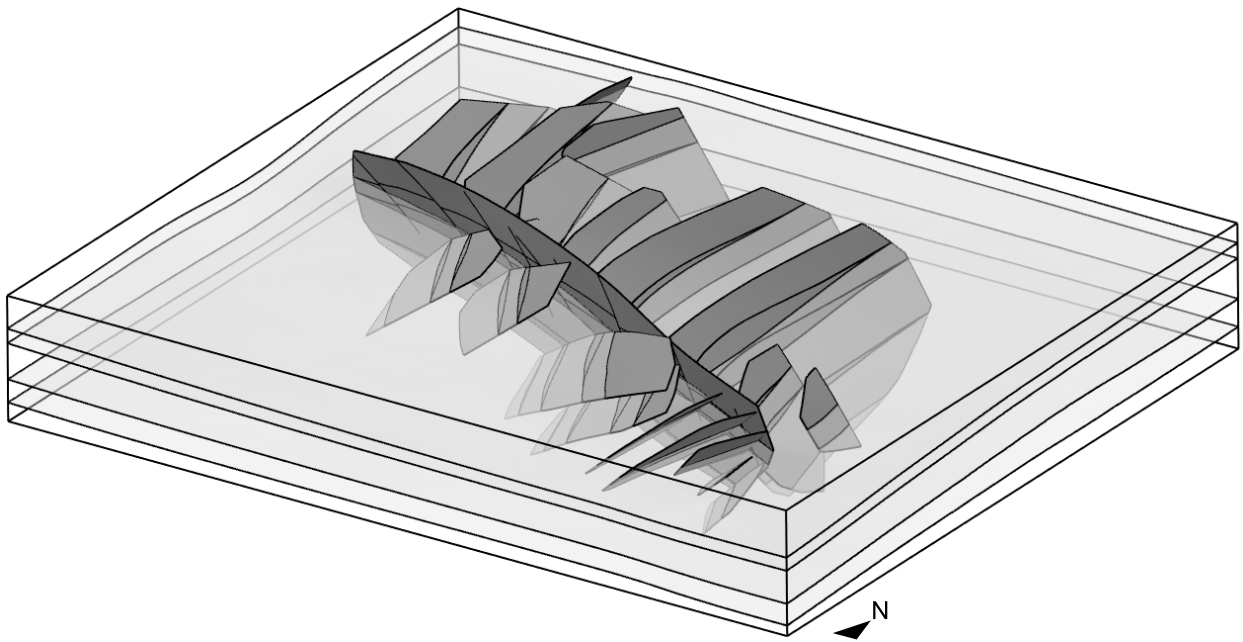


Figure 17: Clyde model with challenging fault contacts

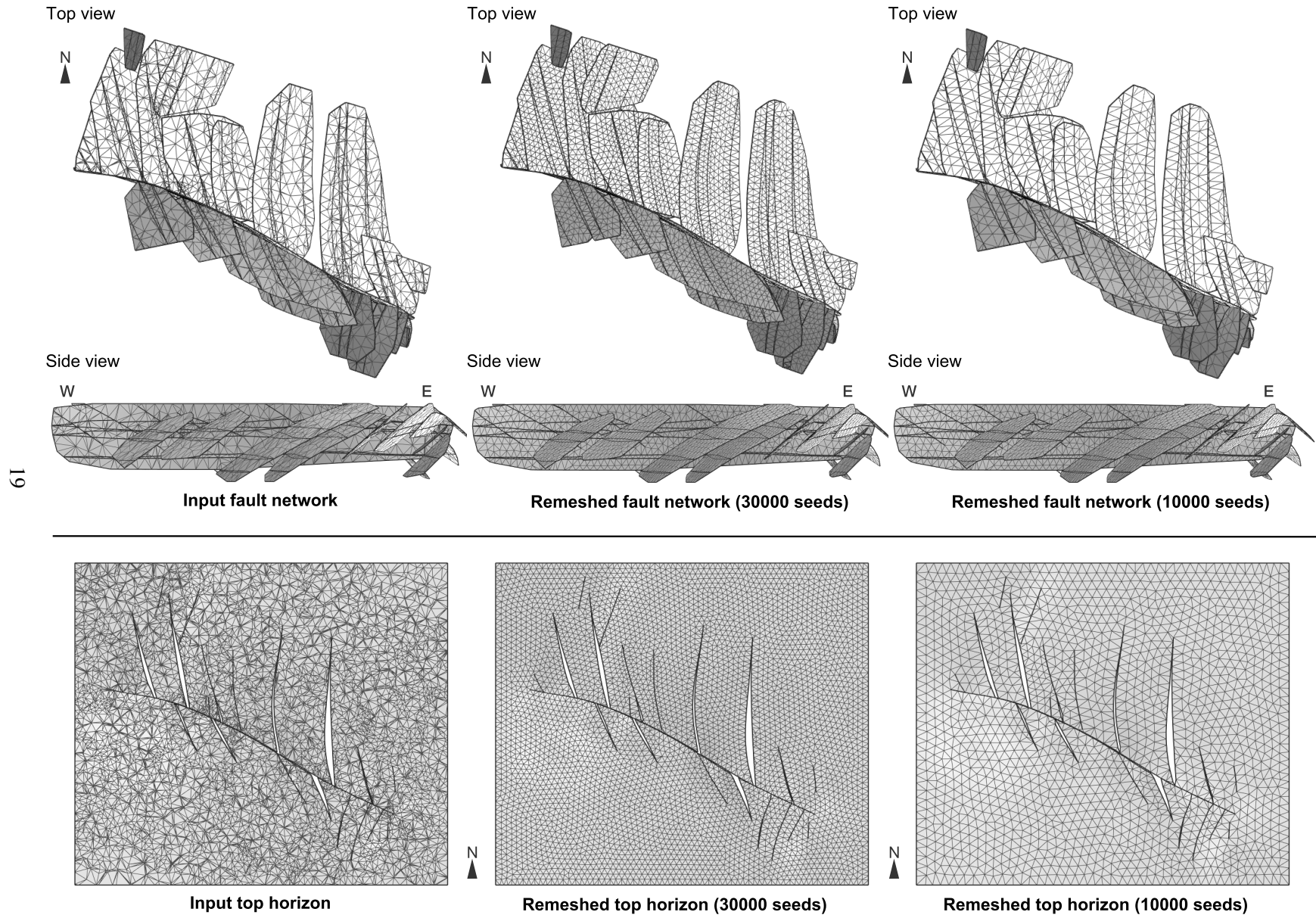


Figure 18: Remeshing the Clyde model with 30000 and 10000 seeds (see Fig. 17). See Tables 1 and 2 for details.

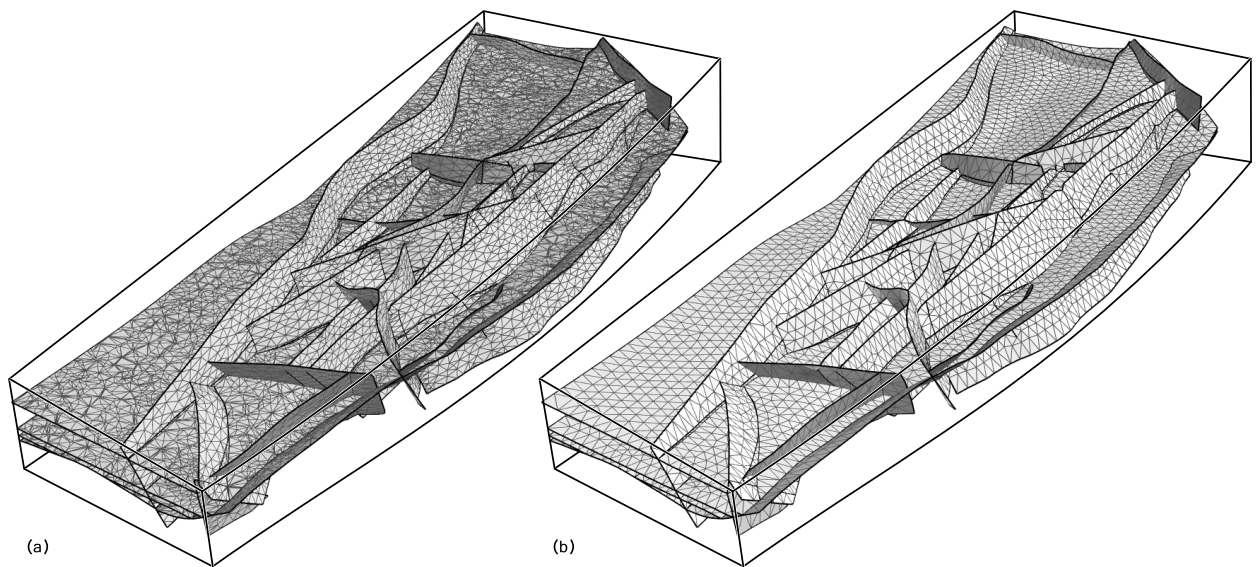
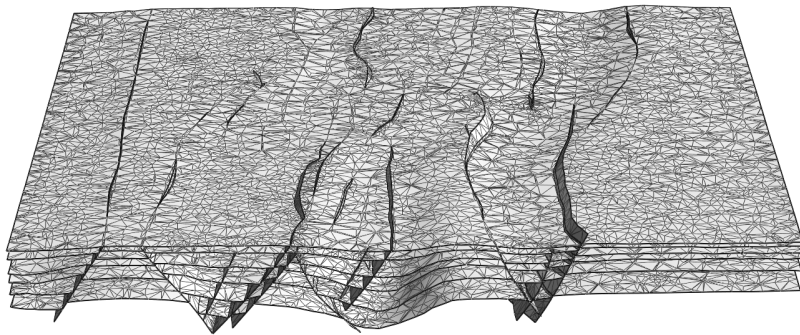
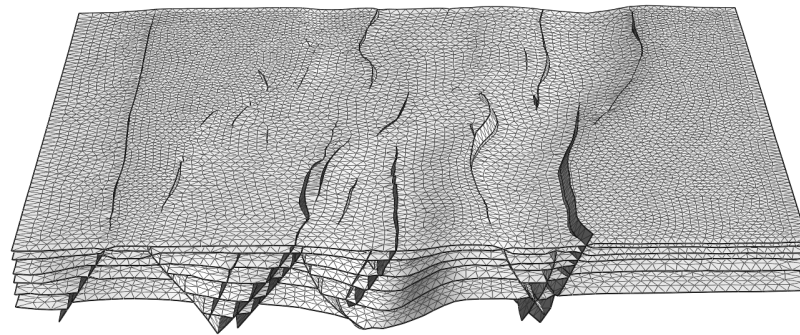


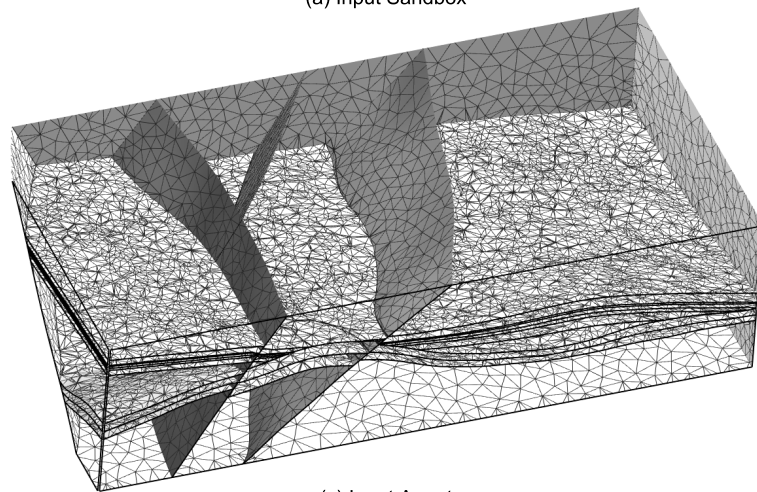
Figure 19: Nancy model remeshing. (a) Input model (b) Model remeshed with 10000 seeds (see Tables 1 and 2 for details).



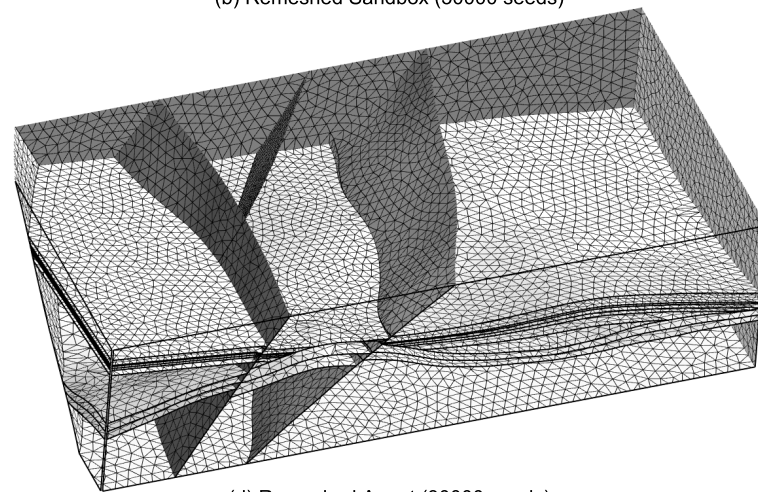
(a) Input Sandbox



(b) Remeshed Sandbox (30000 seeds)



(c) Input Annot



(d) Remeshed Annot (30000 seeds)

Figure 20: Challenging model remeshing: Sandbox and Annot (see Tables 1 and 2 for details)

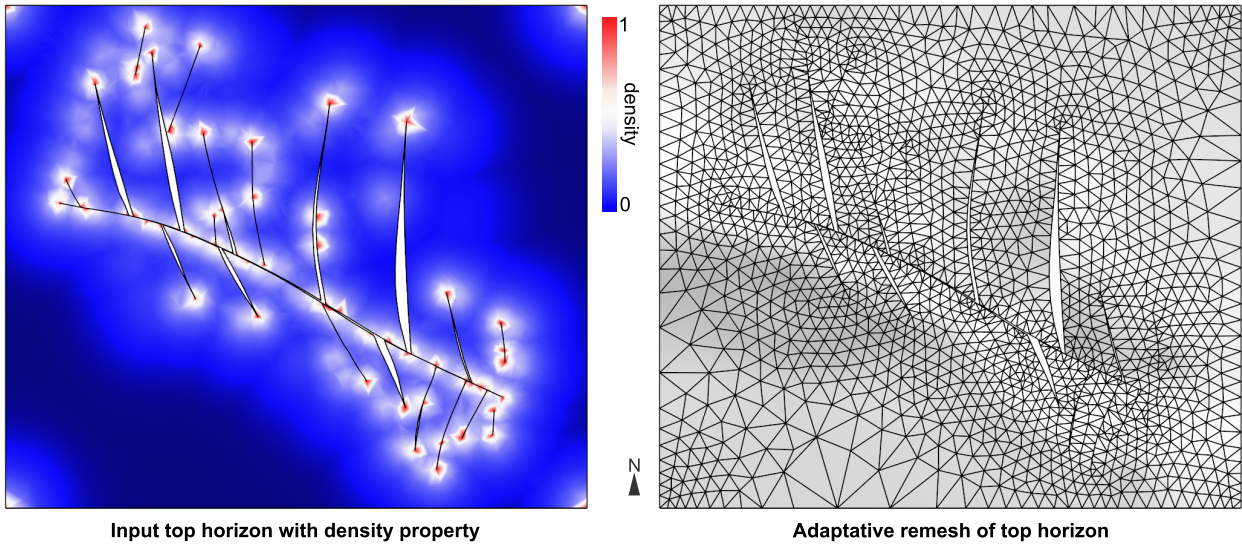


Figure 21: Adaptive remeshing of top horizon in Clyde model. A density property computed from the distance to the triple points of the model  $\rho(y) = (1 - d(y)/d_{max})^4$  was used to obtain an adaptive remesh of the Clyde model with 10000 seeds. Unlike uniform remeshing, the result depends on the input mesh quality because density is interpolated on it.

Dataset	#Seeds	#Vert.	#Trgl	#Surf.	#Lines	#T.Pts	Angles (deg)		Avg qual.	Area (m2)	Timing (s)		Haus. dist. (% bbox diag.)	Bbox diag. (m)
							Min	> 30 (%)			Sampling	Mesh		
<b>Veins</b>	<b>Input</b>	<b>471337</b>	<b>923286</b>	<b>29</b>	<b>0</b>	<b>0</b>	<b>0.01</b>	<b>22.07</b>	<b>0.55</b>	<b>5.20E+08</b>				11069
	1000	19928	35484	29	0	0	1.04	3.46	0.81	5.16E+08	153	33	0.44	11069
<b>Forward</b>	<b>Input</b>	<b>10151</b>	<b>13588</b>	<b>46</b>	<b>76</b>	<b>40</b>	<b>0.01</b>	<b>20.21</b>	<b>0.53</b>	<b>6.63E+04</b>				152.847
	1000	2457	3400	47	71	35	0.56	3.25	0.82	6.61E+04	12	1	1.45	152.847
	5000	7961	12849	46	74	36	1.85	1.00	0.88	6.62E+04	28	1	0.25	152.847
	10000	14096	23845	46	77	41	1.30	0.58	0.89	6.62E+04	46	2	0.18	152.847
<b>Detachment</b>	<b>Input</b>	<b>61480</b>	<b>109098</b>	<b>50</b>	<b>84</b>	<b>46</b>	<b>7.86</b>	<b>2.19</b>	<b>0.79</b>	<b>3.98E+09</b>				36816.7
	15000	25165	44599	50	79	41	2.60	0.50	0.90	3.98E+09	61	3	0.31	36814.9
	30000	42219	76514	50	82	44	3.85	0.24	0.91	3.98E+09	85	3	0.12	36814.8
<b>Leipzig</b>	<b>Input</b>	<b>9286</b>	<b>11344</b>	<b>188</b>	<b>320</b>	<b>166</b>	<b>0.98</b>	<b>7.54</b>	<b>0.73</b>	<b>1.00E+07</b>				1724.07
	5000	8578	11694	186	287	135	4.05	1.61	0.84	1.00E+07	13	1	0.51	1724.07
	10000	14911	22281	186	295	143	6.08	0.96	0.86	1.00E+07	23	2	0.79	1724.07
<b>Lambda</b>	<b>Input</b>	<b>24528</b>	<b>37553</b>	<b>132</b>	<b>256</b>	<b>177</b>	<b>0.09</b>	<b>15.52</b>	<b>0.62</b>	<b>2.57E+08</b>				7814.07
	1000	3416	3711	144	236	147	0.98	8.35	0.73	2.57E+08	20	2	1.17	7814.07
	10000	16113	24223	134	242	155	0.57	1.46	0.86	2.57E+08	33	3	0.374	7814.07
<b>DFN</b>	<b>Input</b>	<b>7876</b>	<b>7723</b>	<b>435</b>	<b>307</b>	<b>481</b>	<b>0.00</b>	<b>40.70</b>	<b>0.33</b>	<b>1.03E+09</b>				18282.6
	30000	38081	62070	435	300	480	1.00	0.88	0.88	1.03E+09	48	3	1.2	18279.6
<b>HC</b>	<b>Input</b>	<b>39919</b>	<b>70684</b>	<b>80</b>	<b>140</b>	<b>80</b>	<b>0.12</b>	<b>19.54</b>	<b>0.60</b>	<b>2.39E+09</b>				23083.6
	30000	37255	65198	80	141	81	0.78	0.25	0.91	2.39E+09	72	5	0.327	23083.6
<b>Cloudspin</b>	<b>Input</b>	<b>18313</b>	<b>30049</b>	<b>97</b>	<b>124</b>	<b>112</b>	<b>0.00</b>	<b>25.59</b>	<b>0.52</b>	<b>8.93E+08</b>				19339.8
	5000	10778	16494	91	117	103	0.45	3.52	0.82	8.92E+08	21	3	0.77	19339.7
	10000	17725	28725	94	134	124	0.30	2.25	0.85	8.92E+08	29	3	0.6	19339.5
<b>Clyde</b>	<b>Input</b>	<b>41355</b>	<b>69343</b>	<b>227</b>	<b>387</b>	<b>303</b>	<b>0.01</b>	<b>20.39</b>	<b>0.56</b>	<b>9.05E+08</b>				15883.8
	10000	15551	23367	206	318	244	0.72	2.51	0.85	9.04E+08	38	4	0.79	15883.8
	30000	38884	64850	220	354	282	0.15	1.30	0.88	9.05E+08	66	9	0.74	15883.8
<b>Nancy</b>	<b>Input</b>	<b>59115</b>	<b>85775</b>	<b>753</b>	<b>1307</b>	<b>774</b>	<b>0.00</b>	<b>25.98</b>	<b>0.50</b>	<b>1.83E+08</b>				13502.4
	10000	24840	30445	719	1096	626	0.13	6.88	0.75	1.83E+08	43	21	0.83	13500.9
	50000	79087	119309	741	1259	774	0.05	2.53	0.84	1.83E+08	106	49	0.27	13502.3
<b>Annot</b>	<b>Input</b>	<b>76204</b>	<b>130403</b>	<b>332</b>	<b>590</b>	<b>300</b>	<b>0.00</b>	<b>20.61</b>	<b>0.56</b>	<b>7.42E+08</b>				12650.5
	3000	12737	18253	301	455	212	0.51	5.69	0.77	7.42E+08	40	7	1.02	12650.5
	20000	41761	68240	311	522	264	0.55	2.31	0.85	7.42E+08	80	10	0.26	12650.5
<b>Sandbox</b>	<b>Input</b>	<b>72927</b>	<b>109267</b>	<b>500</b>	<b>688</b>	<b>713</b>	<b>0.00</b>	<b>21.98</b>	<b>0.53</b>	<b>7.60E+07</b>				4641.93
	30000	52498	77688	503	890	897	0.00	1.11	0.85	7.59E+07	93	28	0.64	4641.93

Table 2: Remeshing result statistics. For each model, input model and produced results are compared in terms of mesh sizes, numbers of components (surfaces, lines, and triple points), and quality (minimum triangle angle, percentage of triangles with an angle inferior to 30 degrees, average quality); the distance between them is measured with the Hausdorff distance.

## 5. Discussion

The surface remeshing method proposed in this paper is completely automatic and performs in several minutes or less on typically sized 3D structural models. It operates both globally and locally on the input model whose surface parts, contact lines, and triple points are remeshed simultaneously depending on the selected resolution. The trade-off of the automation is that a precise control on the performed modifications is not possible in the current implementation. Neither does the method give any formal guarantee on the quality of the output triangles or on the topology of the output model. Both the global optimization and the local analysis of the model have obvious limits. Uniform seed density may induce inside some Voronoi cells. These modifications may be questioned, since they depend on the local placement of a few seeds and may result in the loss of some important geological features. Therefore, a first perspective is to develop strategies to avoid some of the modifications, for example the merger of triple points aligned on a contact line (Fig. 11b). The second one is to adapt seed density so that important features are kept. Varying seed density is already supported by the method since the Centroidal Voronoi Tessellation objective function includes a density function (Equation 2) and the method can generate adaptive meshes (Fig. 21). Adaptive density could also be used to handle object of different scales in a model or curved surfaces.

The main perspective for this method is to adapt it to volumetric meshing, see the preliminary results of Pellerin et al. (2012), and use the generated meshes to solve partial differential equations describing coupled physical processes in the subsurface.

## Acknowledgments

This work has been performed in the frame of the Gocad research project and of the “Investissements d’avenir” Labex RESSOURCES21 (ANR-10-LABX-21). Bruno Lévy is partly supported by the European Research Council (ERC-StG-205963) and the ANR (Morpho). We thank the industry and academic members of the Gocad Research Consortium<sup>1</sup> for supporting this research, and particularly Paradigm Geophysical for providing the Gocad software and API. Thanks to Chevron, Harvard University, IFPEN, Paradigm Geophysical, Schlumberger, and Total for providing data sets. We would also like to thank the anonymous reviewers for constructive comments which helped improve this paper.

## References

- Alliez, P., Colin de Verdiere, E., Devillers, O., Isenburg, M., 2005. Centroidal Voronoi diagrams for isotropic surface remeshing. *Graphical Models* 67 (3), 204231.
- Alliez, P., Ucelli, G., Gotsman, C., Attene, M., 2008. Recent advances in remeshing of surfaces. In: *Shape Analysis and Structuring. Mathematics and Visualization*. Springer Berlin Heidelberg, pp. 53–82.
- Amenta, N., Bern, M., 1999. Surface reconstruction by Voronoi filtering. *Discrete and Computational Geometry* 22 (4), 481–504.
- Andujar, C., Brunet, P., Ayala, D., 2002. Topology-reducing surface simplification using a discrete solid representation. *ACM Transactions on Graphics* 21 (2), 88–105.
- Aspert, N., Santa-Cruz, D., Ebrahimi, T., 2002. Mesh: Measuring errors between surfaces using the hausdorff distance. In: *Multi-media and Expo, 2002. ICME’02. Proceedings. 2002 IEEE International Conference on*. Vol. 1. IEEE, pp. 705–708.
- Aurenhammer, F., 1991. Voronoi diagrams a survey of a fundamental geometric data structure. *ACM Computing Surveys (CSUR)* 23 (3), 345–405.
- Calcagno, P., Chiles, J., Courrioux, G., Guillen, A., 2008. Geological modelling from field data and geological knowledge: Part i. modelling method coupling 3D potential-field interpolation and geological rules. *Physics of the Earth and Planetary Interiors* 171 (14), 147–157.

---

<sup>1</sup><http://www.gocad.org/w4/index.php/consortium/members>

- Caumon, G., Collon-Drouaillet, P., Le Carlier de Veslud, C., Sausse, J., Viseur, S., 2009. Surface-based 3D modeling of geological structures. *Mathematical Geosciences* 41 (9), 927-945.
- Caumon, G., Gray, G. G., Antoine, C., Titeux, M.-O., 2013. 3D implicit stratigraphic model building from remote sensing data on tetrahedral meshes: theory and application to a regional model of La Popa Basin, NE Mexico. *IEEE Transactions on Geoscience and Remote Sensing* 51 (3), 1613–1621.
- Chen, Z., Cao, J., Wang, W., Sep. 2012. Isotropic surface remeshing using constrained centroidal Delaunay mesh. *Computer Graphics Forum* 31 (7pt1), 2077–2085.
- Colin de Verdiere, E., Ginot, G., Goac, X., 2012. Multinerves and helly numbers of acyclic families. In: *Proceedings of the 2012 symposium on Computational Geometry*. ACM, pp. 209–218.
- Colletta, B., Letouzey, J., Pinedo, R., Ballard, J. F., Bale, P., 1991. Computerized x-ray tomography analysis of sandbox models: Examples of thin-skinned thrust systems. *Geology* 19 (11), 1063–1067.
- Collon-Drouaillet, P., Henrion, V., Pellerin, J., 2012. An algorithm for 3D simulation of branchwork karst networks using horton parameters and A-star. application to a synthetic case. *Geological Society of London-Special Publications* 370 (1).
- Dey, T. K., Levine, J. A., 2009. Delaunay meshing of piecewise smooth complexes without expensive predicates. *Algorithms* 2 (4), 1327–1349.
- Du, Q., Faber, V., Gunzburger, M., 1999. Centroidal Voronoi tessellations: Applications and algorithms. *SIAM Review* 41 (4), 637–676.
- Du, Q., Gunzburger, M., Ju, L., 2003. Constrained centroidal Voronoi tessellations for surfaces. *SIAM Journal on Scientific Computing* 24 (5), 1488–1506.
- Dunbar, J. A., Cook, R. W., Jul. 2003. Palinspastic reconstruction of structure maps: an automated finite element approach with heterogeneous strain. *Journal of Structural Geology* 25 (7), 1021–1036.
- Edelsbrunner, H., Shah, N. R., 1997. Triangulating topological spaces. *International Journal of Computational Geometry and Applications* 7 (4), 365–378.
- Farmer, C. L., 2005. Geological modelling and reservoir simulation. In: Iske, A., Randen, T. (Eds.), *Mathematical Methods and Modelling in Hydrocarbon Exploration and Production*. Vol. 7. Springer-Verlag, Berlin/Heidelberg, pp. 119–212.
- Frey, P. J., Borouchaki, H., May 1999. Surface mesh quality evaluation. *International Journal for Numerical Methods in Engineering* 45 (1), 101–118.
- Garland, M., Heckbert, P. S., 1997. Surface simplification using quadric error metrics. In: *Proceedings of the ACM SIGGRAPH Conference on Computer Graphics*. pp. 209–216.
- Guzowski, C. A., Mueller, J. P., Shaw, J. H., Muron, P., Medwedeff, D. A., Bilotti, F., Rivero, C., Apr. 2009. Insights into the mechanisms of fault-related folding provided by volumetric structural restorations using spatially varying mechanical constraints. *AAPG Bulletin* 93 (4), 479–502.
- Laurent, G., 2013. *Prise en compte de l'histoire géologique des structures dans la création de modèles numériques 3D compatibles*. Ph.D. thesis, Université de Lorraine, France.
- Lepage, F., 2003. *Generation de maillages tridimensionnels pour la simulation des phénomènes physiques en géosciences*. Ph.D. thesis, INPL, Nancy, France.
- Levy, B., Bonneel, N., 2013. Variational anisotropic surface meshing with Voronoi parallel linear enumeration. In: Jiao, X., Weill, J.-C. (Eds.), *Proceedings of the 21st International Meshing Roundtable*. Springer Berlin Heidelberg, Berlin, Heidelberg, pp. 349–366.
- Levy, B., Liu, Y., 2010. Lp centroidal Voronoi tessellation and its applications. *ACM Transactions on Graphics (SIGGRAPH conference proceedings)* Patent pending - FR 10/02920 (filed 07/09/10).
- Liu, Y., Wang, W., Levy, B., Sun, F., Yan, D.-M., 2009. On centroidal Voronoi tessellation - energy smoothness and fast computation. In: *ACM Transactions Graphics*. p. 117.
- Lloyd, S., Mar. 1982. Least squares quantization in PCM. *Information Theory, IEEE Transactions on* 28 (2), 129–137.
- Mallet, J.-L., 2002. *Geomodeling*. Oxford University Press, USA.
- Mustapha, H., Dimitrakopoulos, R., Graf, T., Firoozabadi, A., 2011. An efficient method for discretizing 3D fractured media for subsurface flow and transport simulations. *International Journal for Numerical Methods in Fluids* 67 (5), 651–670.
- Nocedal, J., 1980. Updating quasi-Newton matrices with limited storage. *Mathematics of computation* 35 (151), 773–782.
- Pellerin, J., Levy, B., Caumon, G., 2011. Topological control for isotropic remeshing of non-manifold surfaces with varying resolution: application to 3D structural models. In: Marschallinger, R., Zolb, R. (Eds.), *Proc. IAMG, Salzburg*. pp. 678–685.
- Pellerin, J., Levy, B., Caumon, G., Oct. 2012. A Voronoi-based hybrid meshing method. In: *International Meshing Roundtable, Research Notes*.
- Prevost, M., Lepage, F., Durlofsky, L. J., Mallet, J.-L., Oct. 2005. Unstructured 3D gridding and upscaling for coarse modelling of geometrically complex reservoirs. *Petroleum Geoscience* 11 (4), 339–345.
- Rossignac, J. R., Borrel, P., 1993. Multi-resolution 3D approximations for rendering complex scenes. In: Falcidieno, B., Kunii, T. L. (Eds.), *Geometric Modeling in Computer Graphics*. Springer, pp. 455–465.

- Salles, L., Ford, M., Joseph, P., De Veslud, C., Le Solleuz, A., 2011. Migration of a synclinal depocentre from turbidite growth strata: the Annot syncline, SE France. *Bulletin de la Societe Geologique de France* 182 (3), 199–220.
- Valette, S., Chassery, J.-M., Prost, R., 2008. Generic remeshing of 3D triangular meshes with metric-dependent discrete Voronoi diagrams. *IEEE Transactions on Visualization and Computer Graphics* 14 (2), 369–381.
- Yan, D.-M., Levy, B., Liu, Y., Sun, F., Wang, W., 2009. Isotropic remeshing with fast and exact computation of restricted Voronoi diagram. *ACM/EG Symposium on Geometry Processing / Computer Graphics Forum* 28 (5), 1145–1454.
- Zhang, J., Emelianenko, M., Du, Q., 2012. Periodic centroidal Voronoi tessellations. *International Journal of Numerical Analysis and Modeling* 9 (4), 950–969.